JMEPEG (2009) 18:626–630
DOI: 10.1007/s11665-009-9483-x

1059-9495/$19.00

Implementation of the Müller-Achenbach-Seelecke Model for Shape Memory Alloys in ABAQUS

Frank Richter, Oliver Kastner, and Gunther Eggeler

(Submitted September 15, 2008; in revised form April 15, 2009)

Temperature changes caused by latent phase transformation heats are an integral part of the behavior of shape memory alloys. The ensuing thermomechanical coupling between the mechanical and thermal fields is covered by the Müller-Achenbach-Seelecke (MAS) model. Its versatility when implemented as a standalone program has been documented extensively in the literature (S. Seelecke and I. Müller, *Appl. Mech. Rev.*, 57(1), 2004, p 23-46; M. Achenbach, *Int. J. Plast.*, 5(4), 1989, p 371-395; I. Müller and S. Seelecke, *Mathem. Comp. Mod.*, 34(12-13), 2001, p 1307-1355). This model has been evaluated within various simulation environments, standalone programs as well as in commercial tools like FEMLAB and ANSYS. Here we present an application of the MAS model within the finite-element (FEM) simulation software ABAQUS. The MAS constitutive equation of state for SMA is ported into ABAQUS via a user material interface. We present the results of simulation examples using this computer model and validate them by comparison with reference solutions. Using ABAQUS finite elements allowing for temperature as a degree of freedom, the effects of the release and the absorption of latent heats in a fully coupled simulation are demonstrated. Further, a FEM implementation of the model extension to polycrystalline materials is presented as these are of greater relevance with regard to engineering applications. The results show that the incorporation of the MAS model into the ABAQUS environment provides a powerful tool useful in the framework of engineering design studies, especially in situations which require nonisothermal conditions and phase transitions.

Keywords ABAQUS, beam bending, FEM-simulation, Müller-Achenbach-Seelecke model, shape memory alloys, thermomechanical coupling

1. Introduction

Shape memory alloys (SMA) are increasingly being employed as sensors and actuators. To assign them a function their behavior should be accessible to physical interpretation to utmost precision, hence reliable modeling techniques are mandatory. Depending on temperature, the constitutive behavior of SMAs is characterized by either pseudoplasticity (at low temperature) or by pseudoelasticity (at high temperature). Ideally, the constitutive model for a SMA should be so versatile as to be able to capture both pseudoplasticity and pseudoelasticity; hence, accessing the entire range of SMA behavior. The model should reflect the complex, nonlinear hysteretic, and thermomechanically coupled material behavior of SMAs on a physically sound basis.

Thermomechanical coupling is inherent to SMA applications as phase changes are inevitably accompanied by temperature effects caused by latent heat. Consequently, mechanical and thermal equations need to be solved simultaneously. A model capable of this truly thermomechanically coupled approach is the one named after Müller, Achenbach, and Seelecke (Ref 1, henceforth 'MAS model') which reflects all the salient characteristics of SMA. In the original formulation, single-crystalline materials are considered. An extension to polycrystalline materials was recently reported (Ref 13).

The present work summarizes some results obtained by the implementation of this model in the Finite-Element-method (FEM) environment ABAQUS® (ABAQUS, Inc., Dassault Systèmes Simulia Corp., Providence, RI, USA; release 6.7), indicating harmony to reference solutions taken either from alternative implementations of the model or from basic mechanics. Both the single crystal and the polycrystal formulation of the model are considered.

2. MAS Model and FEM Implementation

Crystallographic observations have revealed that a SMA under uniaxial loading exhibits a layered crystalline structure. Thus, the MAS model considers ideal mesoscopic crystal layers in one of the three model phases austenite (A) and two martensitic twin phases (M+, M−) (Ref 1). The model derivation adheres strictly to thermodynamics and roots in the idea of a three-well potential energy with minima indicating the

This article is an invited paper selected from presentations at Shape Memory and Superelastic Technologies 2008, held September 21-25, 2008, in Stresa, Italy, and has been expanded from the original presentation.

Frank Richter, Oliver Kastner, and **Gunther Eggeler**, Department of Materials Science, Institute for Materials, Ruhr-University Bochum, 44780 Bochum, Germany. Contact e-mails: Frank.Richter@ruhr-universitaet-bochum.de, Oliver.Kastner@ruhr-universitaet-bochum.de, and Gunther.Eggeler@ruhr-universitaet-bochum.de.

stable locations of these three phases. The model yields a constitutive equation for the stress σ as a function of external strain ε and the internal variables x_A, x_{M+}, and x_{M-} which express the phase fractions of the model phases,

$$\sigma = E_M \cdot \frac{\varepsilon - (x_{M+} - x_{M-}) \cdot \varepsilon_T}{x_{M+} + x_{M-} + \frac{E_M}{E_A} \cdot x_A}. \quad \text{(Eq 1)}$$

The elasticity of the pure phases is expressed by the Young's moduli E_M and E_A and a martensitic transformation causes a residual strain ε_T. According to the MAS model, the phase fractions are implicitly functions of the temporal evolution of the stress-strain field and the temperature. These are determined by a set of rate equations representing an initial value problem (coupled ODE system) solved numerically for given strain and temperature. The numerically stiff feature of this ODE requires a stable integration scheme for robust solution. Here we use an implicit Runge-Kutta scheme of order five with an adaptive time step size called RADAU IIa (Ref 2). The temperature evolution within the specimen is due to latent heat emission and absorption and the according heat exchange with the ambiance. Assuming temperature homogeneity in simple geometries, the temperature can be calculated from the integral energy balance which represents an additional differential equation to be solved along with the rate equations for the phase fractions. Previously, this was accomplished by a standalone FORTRAN program (Ref 3, 4). An online version of this model considering a SMA wire is illustrated on the Internet (Ref 5).

ABAQUS/Standard allows user implementations of constitutive equations of state through a FORTRAN subroutine called UMAT (User Material), where the state of the nodal field quantities (here, displacements and temperature) can be accessed. UMAT is called by ABAQUS within its own numerical procedure while striving for a converged solution. Here, we have used the UMAT interface to adopt the standalone implementation of the MAS model into the ABAQUS environment. Further, the user has to provide the Jacobian stiffness matrix which for the MAS model reads

$$\frac{d\sigma}{d\varepsilon} = \frac{\partial\sigma}{\partial\varepsilon} + \frac{\partial\sigma}{\partial x_{M+}} \cdot \frac{dx_{M+}}{dt} \cdot \frac{dt}{d\varepsilon} + \frac{\partial\sigma}{\partial x_{M-}} \cdot \frac{dx_{M-}}{dt} \cdot \frac{dt}{d\varepsilon}, \quad \text{(Eq 2)}$$

owing to the dependence of the phase fractions on time t and the identity $x_A = 1 - (x_{M+} + x_{M-})$ (Ref 6, 7) while ε_T is a constant.

Whenever ABAQUS increments the nodal displacements and temperature, the actual evolution of the phase fractions x_A, x_{M+}, and x_{M-} are calculated from the rate equations by the use of the independent ODE solver RADAU. The phase fractions are calculated w.r.t. the nodal displacements fed in by ABAQUS in every iteration during a load step, when the displacements are changed from $u_i(t)$ to $u_i(t + \Delta t) = u_i(t) + \Delta u_i$. For instants τ with $\tau \in [t, t + \Delta t]$ the independent ODE solver then solves an initial value problem for the phase fractions where $u_i(\tau)$ is linearly interpolated between $u_i(t)$ and $u_i(t + \Delta t)$. Upon convergence, the stresses and the latent heat production due to phase transformations are returned to ABAQUS. Thermomechanical coupling is achieved by ascribing the actual specific latent heat production to the ABAQUS variable RPL within UMAT, hence serving as production term to the global energy balance. Within ABAQUS, the internal heat flux is expressed by Fourier's law and the surface heat flux by Dirichlet or Neumann boundary conditions, respectively, as usual. Note that not all of the ABAQUS elements are capable of the thermomechanical coupling. Rather, some elements employed in this study are strictly mechanical beam elements. In such cases, isothermal conditions are imposed.

Table 1 Details on the numerical implementation and performance of the simulation of the polycrystalline wire (Fig. 4 to 6)

ABAQUS	
Spatial discretization	8 × 8 × 4 elements (width × thickness × length)
Element type	C3D8T (8 nodes at the corners of the element, temperature degree of freedom)
Straining	6% strain in 6 s, 94 s hold time, release of strain in 6 s, 94 s hold time (defines the four load steps)
Initial conditions	$x_A = 1$, $x_{M+} = x_{M-} = 0$, temperature $T = 293$ K
Initial time increment	10^{-5} s in all four steps, set by user
Maximum permitted time increment	10^{-2} s (steps 1 and 3), 10^{-1} s (steps 2 and 4); set by user
Convergence criteria	Default ABAQUS values
RADAU	
Dimension of the system	3 (referring to the rate equations for the state variables x_A, x_{M+}, x_{M-})
Relative error tolerance	10^{-6}
Absolute error tolerance	10^{-6}
Initial step size	10^{-3} s

Convergence performance as reported by the ABAQUS status file for this particular simulation: 3136 increments, out of which 3130 converge in one iteration. A time increment of 10^{-1} s was accepted 1872 times during hold times and a time increment of 10^{-2} s was accepted 1196 times during straining and unstraining. The smoothly converged simulation demonstrates the numerical stability of the interplay between ABAQUS and RADAU

The numerical stability of the computer model is achieved by proper choices of the convergence criteria offered by both ABAQUS and the embedded ODE solver. Table 1 provides an overview over the most important quantities as set for the particular simulation explained in Section 3.3.

The FEM-embedded version of the MAS model features advantages of the FEM method as opposed to the standalone version: the deformation is no longer limited to tension, the geometry and spatial discretization are arbitrary, internal heat conduction affects thermal gradients, mechanical and thermal interaction with other parts of the model and the ambiance can be incorporated. At present, verification of the FEM results is restricted to close reproduction of the outcome of the standalone program as well as by an implementation in FEMLAB® (COMSOL AB, Stockholm, Sweden, Ref 7).

3. Results

3.1 Beam Bending

Beam bending is more interesting than simple axial tension as in this case the magnitude and the sign of the uniaxial normal stress vary through the beam thickness. Planar ABAQUS Euler-Bernoulli beam elements are attractive as they feature a single stress and strain component along and parallel to the beam axis. However, the ABAQUS element library does not offer a beam element for coupled temperature-displacement procedures.

In this subsection, we use the ABAQUS Euler-Bernoulli-beam element B23 and restrict all simulations to strictly isothermal conditions. Using this model, the bending of a straight horizontal SMA cantilever is simulated and the results are compared to a reference solution (a) and to the stress contour produced by a hypothetical ideal elastic-plastic material (b). The simulations allow for geometrically nonlinear behavior.

(a) The bending of a straight SMA cantilever which is fully restrained at one end, but loaded by a vertical point force at its free end is presented in Ref 7. Here, the force is defined as a follower load and the constitutive behavior is pseudoplastic according to the temperature set. The initial phase fractions of M+ and M− are equal. Figure 1 depicts the profile of the M+ fraction over the cross section of the beam in three-dimensional space at the instant of maximum deflection. Upon bending, the solution exhibits the typical compression/tension profile of stress for Euler-Bernoulli beams in the elastic regime modulated by pseudoplastic behavior in the transformation regime (Ref 8). Accordingly, the phase fractions of the martensitic variants evolve along the cantilever axis and through the thickness. The M+ fraction increases where the material is subjected to tensile stress (i.e., $y < y$-position of the neutral fiber in Fig. 1) whereas in compressed material parts, the M− fraction is growing at the expense of the M+ fraction. The neutral fiber is indicated by the feet of the respective data points on the (x, y)-plane, showing the actual deflection in this plane. Analogous graphs can be constructed for the M− fraction, the stress and the strain. Such load-induced phase changes and the according formation of martensite plates have indeed been verified experimentally (Ref 9).

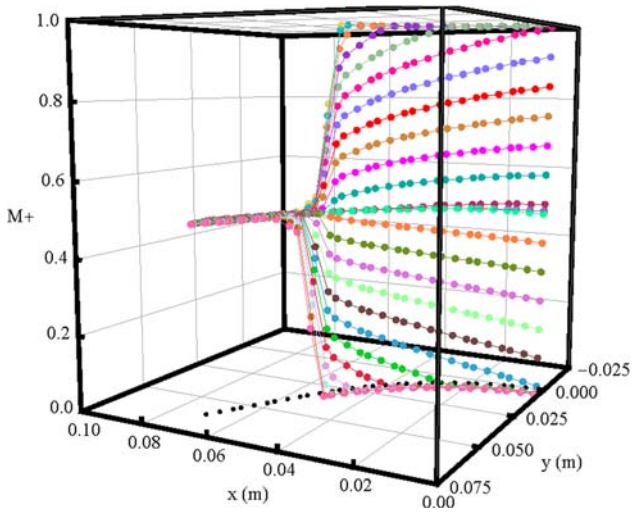

Fig. 1 Spatial distribution of the martensite M+ phase in a cantilever under vertical loading. The straight cantilever is clamped at $x = 0$ in the pseudoplastic state and bent by an external force acting in the positive y-direction at $x = 0.1$ m. Plotted is the spatial distribution of the M+ phase content on and parallel to the beam axis as a function of spatial coordinates at the instant of maximum bending. The spatial resolution through the beam thickness is provided by 27 section points equidistant through the thickness. The *black dots* on the base plane show the beam curvature. Original beam dimensions: Length = 0.1 m, thickness = 0.01 m (Ref 7)

(b) The FEM solution for the transformation zone in a SMA cantilever can be compared to an analytical solution of the yield zone in an ideal elastic-plastic material (Ref 10). Figure 2 shows the solutions for the SMA model and the ideal elastic-plastic cantilever. Both theories predict the same boundary line of the transformed zone (solid black line in Fig. 2) thus verifying the numerical validity of the computer model. Note the analytical solution is capable of this boundary line only while the MAS model additionally provides the spatial distribution of the M+ phase. Both solutions were calculated on the basis of the geometrically nonlinear theories.

3.2 Torsion of a Pseudoelastic SMA Tube

Conveniently, torsion is characterized by a uniaxial state of torque stress. The free oscillation of a pseudoelastic SMA pendulum at constant temperature ($T = 353$ K) has been studied in Ref 11 and 12 using the standalone implementation of the MAS model. We adopt the setting from Ref 11 to study the behavior of the FEM-based computer model where the earlier results serve as reference solution. The torsion pendulum is represented by a thin-walled pseudoelastic NiTi tube (2 mm diameter, 5 cm length, 50 μm wall thickness). Supported at one end, this tube is attached to a weight at the opposite end which produces the required inertia upon free oscillation. The oscillation started from a pre-twisted state where the according torque induces a purely martensitic state. In the FEM-based model, the tube is discretized by 10 ABAQUS beam B33 elements along the axis. The FEM-based solution and the

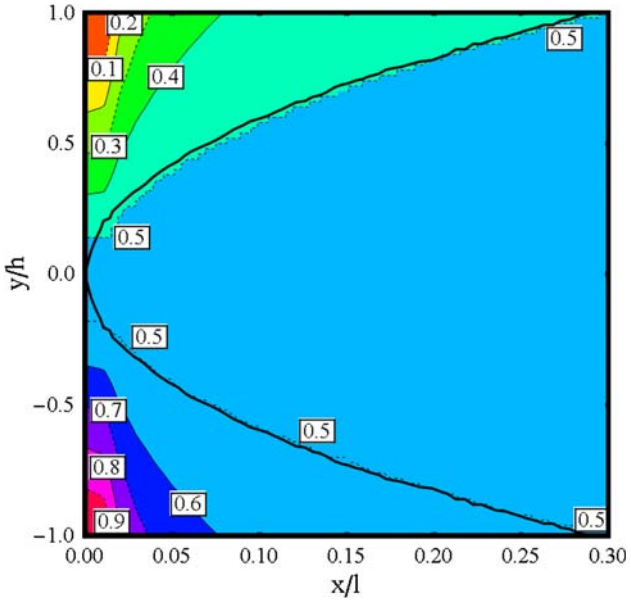

Fig. 2 Contour plot of the M+ fraction (plotted on the undeformed configuration; only 30% of the beam from the clamped end are depicted), defining the transformation zone in a pseudoplastic cantilever at vertical tip loading in the positive y-direction. The load equals 1.825 times the yield load as detected for the geometrically linear case. The *black solid line* indicates the analytical solution for the plastic deformation boundary obtained from an ideally elastic-plastic material (digitized from Ref 10)

reference solution are superposed in Fig. 3 where the black dots indicate the reference solution and lines reflect the FEM-based torsion at three axial nodes (located at the tube ends and in the center, respectively) as function of time. The reference solution coincides with the torsion/time function of the node at the oscillating tube end. At the center node, the torsion is proportionally less while the opposite end remains at rest. During the first 50 s, the inertia of the weight produces sufficient torque to loop the material through the pseudoelastic hysteresis. Accordingly, hysteresis-related energy dissipation causes the significant damping visible in Fig. 3. Eventually, the material behaves purely elastic, effecting undamped harmonic oscillations.

3.3 Tensile Test of a Polycrystalline SMA Wire

Seelecke and Heintze (Ref 13, 14) have contributed a polycrystalline formulation of the MAS model which overcomes some of the physical limitations of the original single-crystalline model. Their method of 'parameterization' renders the model more flexible but preserves the computational simplicity of the single crystal implementation with minor adaptations. The polycrystal model takes into account the averaged excess stresses occurring in a domain-structured material (originating from grain orientations, local transformation stresses, and other local effects). It has been ported into the ABAQUS environment and was used to simulate uniaxial straining of a pseudoelastic SMA wire. The results are compared to the original work (Ref 13). The FEM model employs the ABAQUS element type C3D8T to discretize a wire with dimensions 1.07 mm × 0.8 mm × 6.35 cm (width × thickness × length). This element type is capable of 3D problems, but for the special case of uniaxial loading the application of the one-dimensional polycrystalline MAS model is possible. The significant advantage of the C3D8T element over the formerly used beam-type elements is that this element type permits true thermomechanical coupling. Figures 4 to 6 show the result of such tensile testing with a tetragonal wire geometry. The wire is loaded and unloaded in displacement control mode so as to simulate a complete pseudoelastic loading cycle, see inset in Fig. 4. Temperature effects occur during yielding (0-6 s) and recovery (100-106 s) of the transformation strain (see Fig. 4, inset), where the release and the absorption of latent transformation heat cause self-heating and self-cooling, respectively. These effects are compensated by heat exchange with an ambient medium at a temperature of 293 K. The temperature profile resulting from these heat transfers is resolved in the simulation: Fig. 5 shows a contour plot of the temperature field at the tip face of the wire at maximum load (after 6 s). Note the minute thermal conductivity was chosen deliberately to create a notable thermal gradient throughout the tiny volume of the wire. Figure 4 shows the temperature evolution at three node sets which are localized along the volume center, one face center, and one edge of the wire (incorporating all nodes along the length). Even though

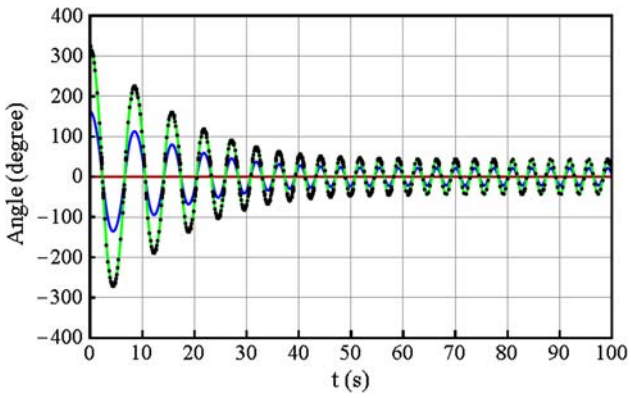

Fig. 3 Free oscillation of a pseudoelastic NiTi torsion pendulum. Comparison of a reference solution from the literature (*black dots*, Fig. 3 in Ref 11) with the FEM-embedded version of the MAS model (*colored lines*). Initially the pendulum is twisted by 324°. *Red line*: Fixed tube end (no angular displacement), *blue line*: node at mid-length, *green line*: torqued end. The reference solution refers to the latter; the red and blue solutions illustrate the axial evolution of the torsion

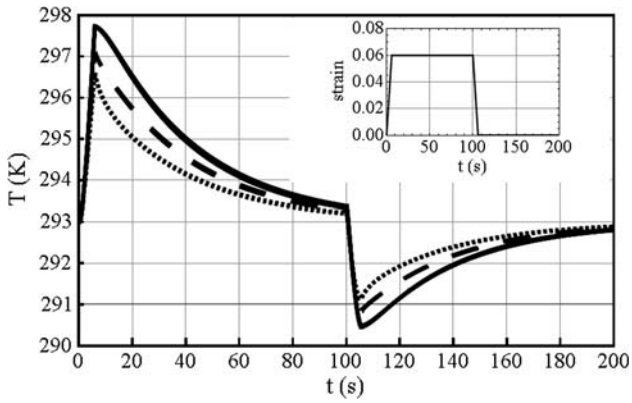

Fig. 4 Temperature as a function of time for three node sets located at the volume center (*solid line*), face center (*dashed line*), and edge (*dotted line*). Inset: imposed strain as function of time

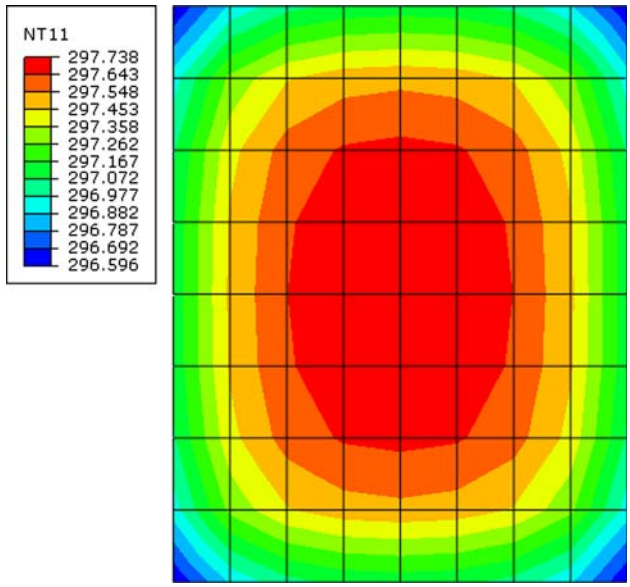

Fig. 5 Contour plot of the temperature field ('NT11,' in K) at the tip of the fully transformed wire at maximum load (after 6 s in Fig. 4), showing a pronounced temperature gradient which indicates the internal heat flux

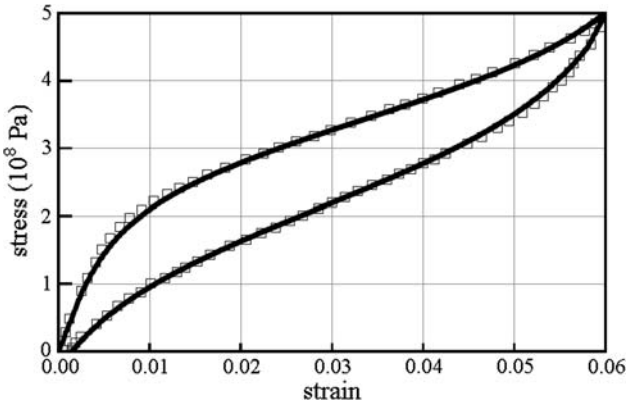

Fig. 6 Simulated stress/strain curve of a pseudoelastic, tetragonal SMA wire under uniaxial straining. *Black dots*: FEM-based simulation, *squares*: reference solution taken from the literature (Fig. 4.11 in Ref 13)

the detected temperature variations are small, the heat flux driven by latent heat produces a distinct temperature field with notable gradients. Such effects are augmented in special geometric situations, under fast straining or, e.g., in composite materials where the heat flow could be restricted. The according stress-strain curve for this example of a polycrystalline model is shown in Fig. 6. Obviously, the FEM-embedded version of the model exhibits convincing coincidence with results obtained by the standalone version of the polycrystalline model in the literature.

4. Conclusions

The ABAQUS-version of the MAS model is capable of achieving a good match to digitized data from reference solutions or, where applicable, to analytical computations. In summary, it can be stated that the MAS model is well suited to describe the constitutive behavior of SMA for both model formulations, single and polycrystalline materials. A prime advantage is its versatility, including the inherent thermomechanical coupling and the extension to polycrystalline materials.

Acknowledgments

Financial support by the German Research Foundation (DFG) Grant no. KA 2304/2-1 is much appreciated. We thank Prof. S. Seelecke (North Carolina State University, USA) and O. Heintze (PhD, German Aerospace Center (DLR), Braunschweig, Germany) for valuable discussions about the model.

References

1. S. Seelecke and I. Müller, Shape Memory Alloy Actuators in Smart Structures: Modeling and Simulation, *Appl. Mech. Rev.*, 2004, **57**(1), p 23–46
2. E. Hairer and G. Wanner, *Solving Ordinary Differential Equations II: Stiff and Differential-Algebraic Problems*, Springer Series in Computational Mathematics 14, 2nd ed., Springer, Berlin, 1996
3. M. Achenbach, A Model for an Alloy with Shape Memory, *Int. J. Plast.*, 1989, **5**(4), p 371–395
4. I. Müller and S. Seelecke, Thermodynamic Aspects of Shape Memory Alloys, *Math. Comp. Mod.*, 2001, **34**(12–13), p 1307–1355
5. Interactive Webpage for the Simulation of Shape Memory Wires, www.smaterial.com
6. J.P. Frautschi, "Finite Element Simulations of Shape Memory Alloy Actuators in Adaptive Structures," M.Sc. Thesis, North Carolina State University, USA, 2003
7. Q. Li, "Modeling and Finite Element Analysis of Smart Materials," Ph.D. Thesis, North Carolina State University, USA, 2006
8. T. Atanackovic and M. Achenbach, Moment-Curvature Relations for a Pseudoelastic Beam, *Cont. Mech. Thermodyn.*, 1989, **1**(1), p 73–80
9. J. Rejzner, C. Lexcellent, and B. Raniecki, Pseudoelastic Behaviour of Shape Memory Alloy Beams Under Pure Bending: Experiments and Modelling, *Int. J. Mech. Sci.*, 2002, **44**(4), p 665–686
10. H. Parisch, Large Displacement of Shells Including Material Nonlinearities, *Comput. Meth. Appl. Mech. Eng.*, 1981, **27**(2), p 183–214
11. O. Heintze, O. Kastner, H. Sahota, and S. Seelecke, The Role of Thermomechanical Coupling in the Dynamic Behavior of Shape Memory Alloys, *IUTAM Symposium on Smart Structures and Structronic Systems: Proceedings of the IUTAM Symposium*, Magdeburg, Germany, U. Gabbert and H.S. Tzou, Ed., Sept 26–29, 2000, Springer, 2001, p 145–152
12. S. Seelecke, Modeling the Dynamic Behavior of Shape Memory Alloys, *Int. J. Non-Lin. Mech.*, 2002, **37**, p 1363–1374
13. O. Heintze, "A Computationally Efficient Free Energy Model for Shape Memory Alloys—Experiments and Theory," Ph.D. Thesis, North Carolina State University, USA, 2004
14. O. Heintze and S. Seelecke, A Coupled Thermomechanical Model for Shape Memory Alloys—From Single Crystal to Polycrystal, *Mater. Sci. Eng. A*, 2008, **481–482**, p 389–394